Supplementary Information

Non-stoichiometric hybrid halide perovskite film for gaseous NH_3 and HCl sensing

Guishun Li,[a] Guangning Hou,[b] Xinghan Zhang,[a] Chongyu Yu,[a] Dianrong Han,[a] Chengbin Jing,*[b] and Junhao Chu [b]

[a] School of Physics and Information Engineering, Jiangsu Second Normal University, Nanjing 211200, China.
[b] Engineering Research Center for Nanophotonics and Advanced Instrument of Ministry of Education; Key Laboratory of Polar Materials and Devices (Ministry of Education); School of Physics and Electronic Science, East China Normal University, Shanghai 201100, China.

Corresponding author: cbjing@ee.ecnu.edu.cn (Chengbin Jing).

Experimental Section

Materials

Lead iodide (PbI_2, 98%) and Hydroiodic acid (HI, in water 55-58%) are purchased from Macklin. Methylamine (33 wt % in absolute ethanol) and Hydrochloric acid (HCl, AR, 36.0 ～ 38.0%) are purchased from Sinopharm Chemical Reagent. The Au-interdigital electrode Al_2O_3-substrates (size: 10×5 mm^2, electrode spacing: 100 μm) are purchased from Changchun Beirun Electronic Technology Co., Ltd. The substrates were cleaned consecutively in acetone, isopropanol, and ethanol ultrasonic bath for 10 min each, and dried under 100 ºC, finally treated with plasma cleaner for 5 min before use.

Material synthesis

Methylammonium iodide (MAI)

MAI was synthesized by mixing methylamine (40 wt. % in water) with HI solution in a 1:1.2 mole ratio in ambient atmosphere at 0˚C for 2 hours. The MAI solution was crystallized in a roto-evaporator at 50°C. The precipitate was washed several times with diethyl ether and then dried at 60˚C in a vacuum oven overnight.

$MAPbI_3$ film preparation

Non-stoichiometric $MAPbI_3$ precursors were prepared by dissolving the MAI and

$PbBr_2$ in DMF with different PbI_2/MAI (MAI: 0.7 M) molar ratios of 0.8:1, 0.9:1, 1:1, 1.1:1, 1.2:1, and 1.3:1, respectively. For the deposition of films, the above precursor solutions were dripped onto Au electrode-containing Al_2O_3-substrates, respectively, which was followed by spin-coating at 3000 rpm for 40 s. Finally, the perovskite films were formed by annealing at 100 °C for 15 min.

Characterization

The crystal phases of perovskite $MAPbI_3$ films were measured using X-ray diffractometer (XRD, PANalytical Empyrean, Cu K_α radiation source at λ =0.15418 nm) under 40 kV and 40 mA in the range $5^o<2\theta<50^o$ at a speed of 10^o min^{-1}. The surface morphologies of films were determined by scanning electron microscope (SEM, Zeiss Gemini 450). Diffuse reflectance spectra were recorded using UV-vis-NIR spectrophotometer (Shimadzu UV2600).

Gas sensing measurement

Gas-sensing experiments were carried on a gas sensing measurement (WS-30A, ZhengZhou Winsen Technology Co., Ltd.) with an 18 L (30×30×20 cm^3) gas chamber. The concentration of NH_3 and HCl were controlled by evaporating proper ammonia solution (25 wt%) and hydrochloric acid solution (37 wt%) on a heater in the chamber, respectively. The sensing performance of perovskite-based sensors was measured and the corresponding gas response was calculated from $(\text{Response}) = (R_g - R_a)/R_a \times 100\%$, where R_a and R_g are the resistances measured in air and target gas atmosphere, respectively. The response/recovery time is defined as the time required for the sensor to reach 90% of the final signal for a given concentration of NH_3 gas. All sensing measurements were carried at room temperature (20~25 ºC) with 50-60% RH.

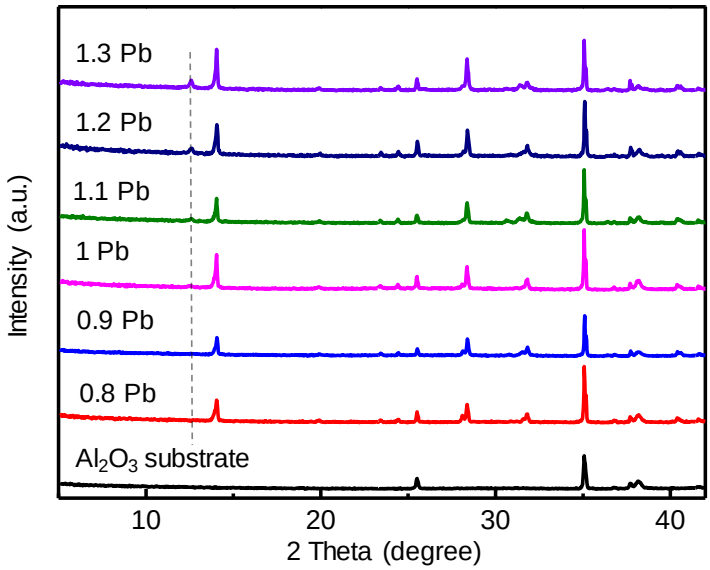

Fig. S1 XRD patterns of non-stoichiometric perovskite $MAPbI_3$ films.

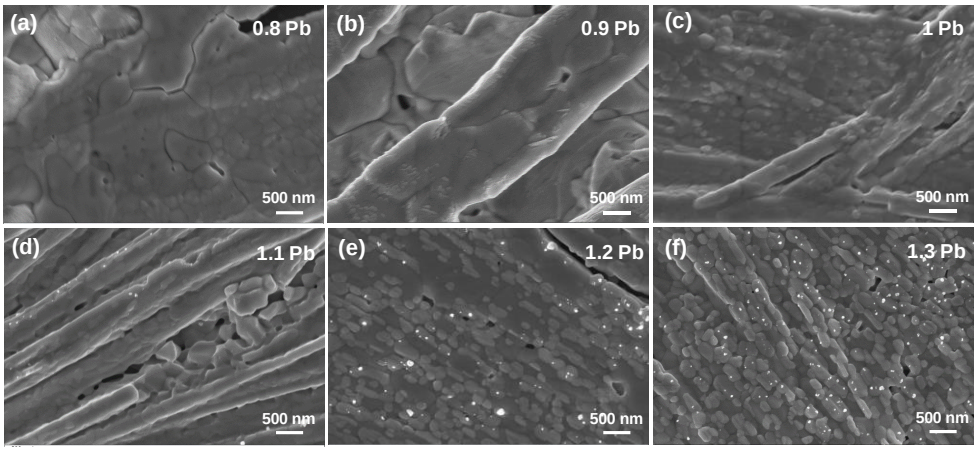

Fig. S2 SEM morphologies of non-stoichiometric perovskite films.

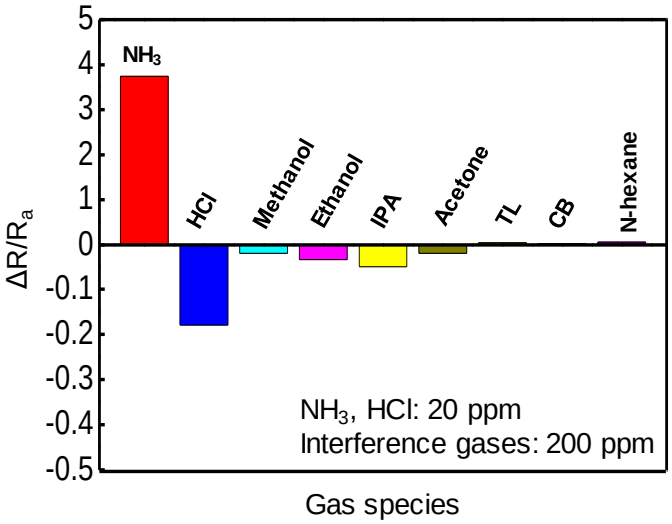

Fig. S3 Gas selectivity of the 1.2Pb-based $MAPbI_3$ sensor toward 20 ppm NH_3/HCl, and other interference gases with 300 ppm.

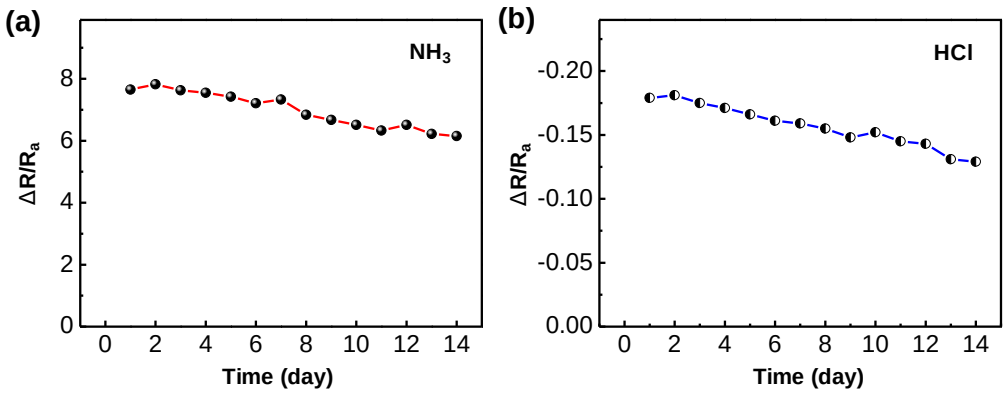

Fig. S4 Long-term stability test of the 1.2Pb-based $MAPbI_3$ sensor. (a) 50 ppm NH_3, (b) 20 ppm HCl. It should be noted that the sample is normally placed in the open atmosphere (20 °C, 45-55%RH) without any protection. There are gradual decline trends in both NH_3 and HCl responses, implying an environmentally sensitive behavior of the film. This degradation is comparable to that of previously reported other perovskite-based sensors. [1, 2] The degradation may be attributed to the oxygen and water vapour in the air. [3, 4] In the further study, the stability of perovskite films would be improved by introducing other components or passivation layers.

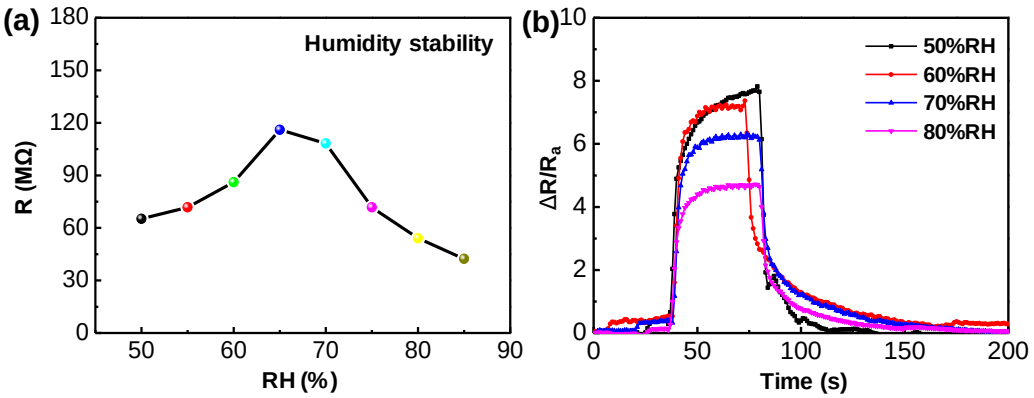

Fig. S5 Humidity stability of 1.2Pb-based sensor. (a) Resistance change of the sensor under different RH, (b) NH_3 response of the sensor under different RH. As previously reported, small amount of water molecules can induce a formation of a hydrated layer on the perovskite crystal, which has an insulating effect resulting in an increase of resistance.[5] In the case of high humidity environment, excess water molecules would trigger proton conduction by water-assisted deprotonation of MA^+ to MA, leading to a rapid drop of resistance.[6] In Fig. S5b, the NH_3 gas response drops gradually as the RH increases. We speculate that a large number of water molecules may be adsorbed on the surface of the film, occupying the reaction sites, and then resulting in a decrease in gas-sensing performance.

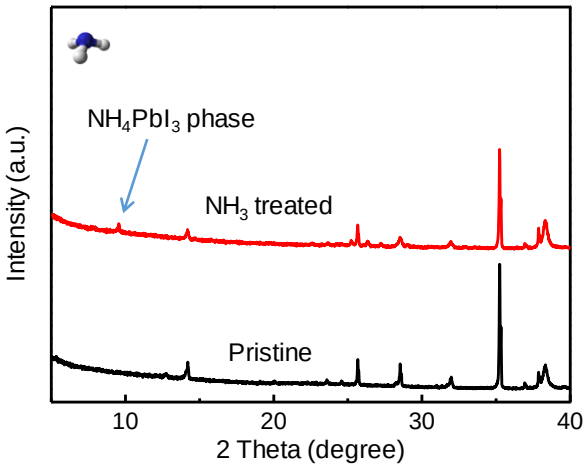

Fig. S6 XRD patterns of the 1.2Pb-based $MAPbI_3$ film before and after NH_3 treatment. One new diffraction peak appears at 9.6°, corresponding to the NH_4PbI_3 phase.[7, 8] It suggests that NH_3 molecules can induce a phase transformation of $MAPbI_3$ into the NH_4PbI_3 by A-site cation replacement.

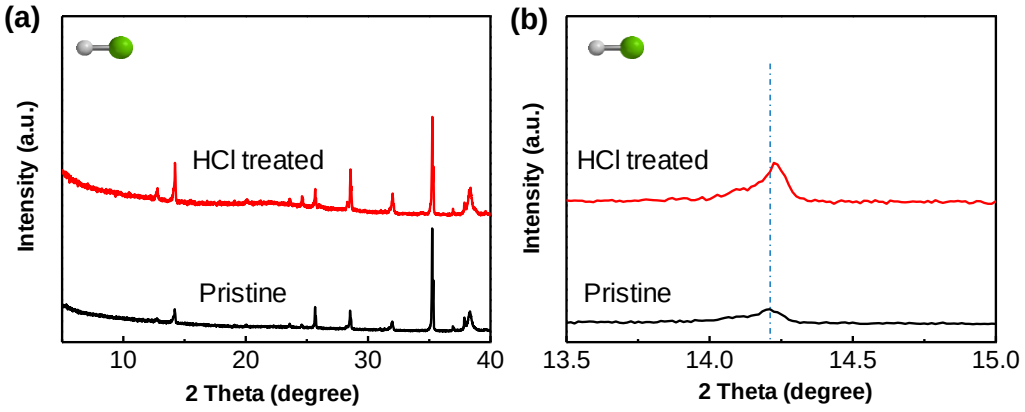

Fig. S7 (a) XRD patterns of the 1.2Pb-based $MAPbI_3$ film before and after HCl vapour treatment, (b) enlarged XRD patterns from 13.5° to 15.0°. A slight right-shift appears obviously when focusing on the enlarged XRD patterns (see Fig. S7b), which is attributed to Cl (small radius) substitution in the $MAPbI_3$ structure during the gaseous anion-exchange. [9]

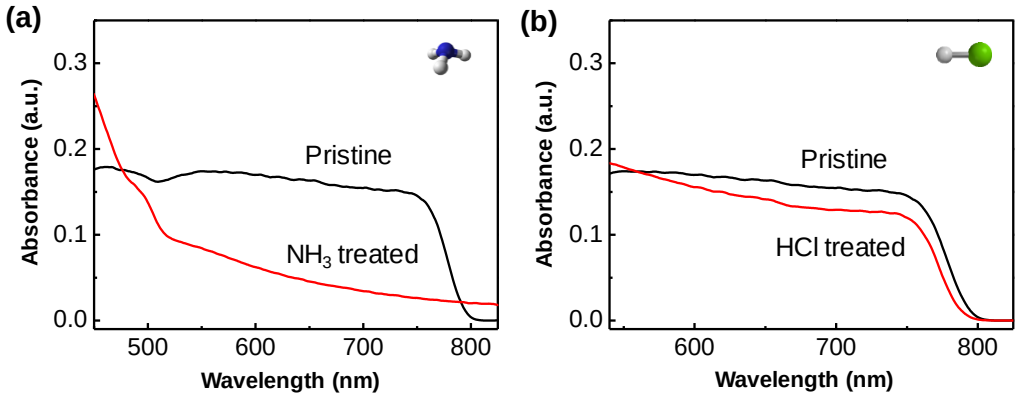

Fig. S8 Evolution of the absorption spectra of the 1.2Pb-based $MAPbI_3$ film upon vapour treatment. (a) NH_3 vapour, (b) HCl vapour. The absorption spectra of the films (Figure S1b) were transformed from the diffuse reflectance spectra by using the Kubelka–Munk function.[10, 11] In the case of NH_3 treatment, the pristine sample has the sharp absorption edge at 750-800 nm, and absorbs strongly below 600 nm; after NH_3 treatment, the intensity of the absorption spectrum is severely decreased, implying a decomposition of $MAPbI_3$ crystal structure, which can be used as a supporting evidence of NH_3-induced phase transformation of $MAPbI_3$. In the case of HCl treatment, there is

an obvious blue-shift change in absorption band edge of the sample upon treatment with HCl vapour, indicative of an occurrence of mixed perovskite $MAPbI_xCl_{3-x}$.

Table S1. Gas sensing properties of the present PbI_2-rich $MAPbI_3$ sensor compared to those of other reported gas sensors.

Target gas	Materials	Concentration (ppm)	Response	Response/ Recovery time (s)	LOD (ppm)	Ref.
NH_3	TiO_2 nanorod array	50	$\triangle R/R_g$=0.61	63/12	/	Zhao et al. (2020)[12]
	MoO_3/SnO_2*	100	R_a/R_g=12.7	13/2	0.01	Liu et al. (2021)[13]
	MXene/TiO_2	10	$\triangle R/R_g$=0.07	76/62	/	Sardana et al. (2022)[14]
	$MAPbI_3$	20	$\triangle R/R_a$=0.96	10/-	0.01	Maity et al. (2021)[15]
	$MAPbI_3$ (rough substrate)	10	$\triangle R/R_a$=1.2	10/12	/	Li et al. (2021)[16]
	$Cs_3Bi_2I_6Br_3$	50	R_a/R_g=2	20/120	/	Jiao et al. (2022)[17]
HCl	$CsPbBr_3$	5	$\|\Delta\lambda\|$ = 0.36 nm (1500 s)	/	1.12	Markina et al. (2023)[18]
NH_3 HCl	Pb-rich $MAPbI_3$	10 20	$\triangle R/R_a$=1.5 $\triangle R/R_a$=0.18	51/16 14/25	0.08 0.11	**This work**

Note: * indicate working temperature at 280℃.

In the case of NH_3 sensing, metal oxide-based gas sensors possess high environmental stability, such as TiO_2 and MoO_3.[12, 13] Nevertheless, many of these sensors suffer from relatively low gas response at room temperature, or require high working temperature to generate oxygen vacancies for an enhancement of gas sensitivity. High operating temperature may be detrimental to the long-term stability of sensor device, and also increase power consumption. In comparison, the halide perovskite materials are sensitive to external stimuli at room temperature such as $MAPbI_3$, $CsPbBr_3$, and lead-free $Cs_3Bi_2I_6Br_3$, indicative of the potential in gas sensor applications. However, there is still much room for improvement in sensor performance. In our as-fabricated 1.2Pb-based sensor, it presents considerable NH_3 response, compared to that of the pristine $MAPbI_3$-based sensor.

In the case of HCl sensing, there are a few related reports. One representative study about fluorescence perovskite $CsPbBr_3$-based HCl sensor is published recently.[18] The detection of HCl gas is realized by fluorescence peak shift of $CsPbBr_3$ nanowire laser. Considering the use of expensive equipment, it may be not suitable to the practical

sensing applications. In contrast, the low-cost resistance-typed 1.2Pb-based sensor presented in our work also possesses superior HCl sensing characteristics.

References

[1] Chen H., Zhang M., Xing B., Fu X., Bo R., Mulmudi H. K., Huang S., Ho-Baillie A. W. Y., Catchpole K. R., Tricoli A. Superior self-charged and-powered chemical sensing with high performance for NO_2 detection at room temperature [J]. Advanced Optical Materials, 2020, 8(11): 1901863.

[2] Huang H., Hao M., Song Y., Dang S., Liu X., Dong Q. Dynamic passivation in perovskite quantum dots for specific ammonia detection at room temperature [J]. Small, 2020, 16(6): e1904462.

[3] Aristidou N., Eames C., Sanchez-Molina I., Bu X., Kosco J., Islam M. S., Haque S. A. Iodide vacancies, fast oxygen diffusion and iodide defects mediate oxygen-induced degradation of perovskite solar cells [J]. Nature Communications, 2017, 8: 15218.

[4] Kim M.-C., Ahn N., Lim E., Jin Y. U., Pikhitsa Peter v., Heo J., Kim S. K., Jung H. S., Choi M. Degradation of $CH_3NH_3PbI_3$ perovskite materials by localized charges and its polarity dependency [J]. Journal of Materials Chemistry A, 2019, 7(19): 12075-12085.

[5] Leguy A. M. A., Hu Y., Campoy-Quiles M., Alonso M. I., Weber O. J., Azarhoosh P., Van Schilfgaarde M., Weller M. T., Bein T., Nelson J., Docampo P., Barnes P. R. F. Reversible hydration of $CH_3NH_3PbI_3$ in films, single crystals, and solar cells [J]. Chemistry of Materials, 2015, 27(9): 3397-3407.

[6] Müller C., Glaser T., Plogmeyer M., Sendner M., Döring S., Bakulin A. A., Brzuska C., Scheer R., Pshenichnikov M. S., Kowalsky W., Pucci A., Lovrinčić R. Water infiltration in methylammonium lead iodide perovskite: Fast and inconspicuous [J]. Chemistry of Materials, 2015, 27(22): 7835-7841.

[7] Huang W., Manser J. S., Sadhu S., Kamat P. V., Ptasinska S. Direct observation of reversible transformation of $CH_3NH_3PbI_3$ and NH_4PbI_3 induced by polar gaseous molecules [J]. The Journal of Physical Chemistry Letters, 2016, 7(24): 5068-5073.

[8] Ruan S., Lu J., Pai N., Ebendorff-Heidepriem H., Cheng Y.-B., Ruan Y., Mcneill C. R. An optical fibre-based sensor for the detection of gaseous ammonia with methylammonium lead halide perovskite [J]. Journal of Materials Chemistry C, 2018, 6(26): 6988-6995.

[9] Chen X., Hu H., Xia Z., Gao W., Gou W., Qu Y., Ma Y. $CsPbBr_3$ perovskite nanocrystals as highly selective and sensitive spectrochemical probes for gaseous HCl detection [J]. Journal of Materials Chemistry C, 2017, 5(2): 309-313.

[10] Singh P., Rana P. J. S., Dhingra P., Kar P. Towards toxicity removal in lead based perovskite solar cells by compositional gradient using manganese chloride [J]. Journal of Materials Chemistry C, 2016, 4(15): 3101-3105.

[11] Gautier R., Massuyeau F., Galnon G., Paris M. Lead halide post-perovskite-type chains for high-efficiency white-light emission [J]. Advanced Materials, 2019, 31(14): e1807383.

[12] Zhao G., Xuan J., Gong Q., Wang L., Ren J., Sun M., Jia F., Yin G., Liu B. In situ growing double-layer TiO_2 nanorod arrays on new-type FTO electrodes for low-concentration NH_3 detection at room temperature [J]. ACS Applied Materials & Interfaces, 2020, 12(7): 8573-8582.

[13] Liu Y., Yuan Z., Zhang R., Ji H., Xing C., Meng F. MoO_3/SnO_2 nanocomposite-based gas sensor for rapid detection of ammonia [J]. IEEE Transactions on Instrumentation and Measurement, 2021, 70: 1-9.

[14] Sardana S., Kaur H., Arora B., Aswal D. K., Mahajan A. Self-powered monitoring of ammonia using

an MXene/TiO_2/cellulose nanofiber heterojunction-based sensor driven by an electrospun triboelectric nanogenerator [J]. ACS Sensors, 2022, 7(1): 312-321.

[15] Maity A., Mitra S., Das C., Siraj S., Raychaudhuri A. K., Ghosh B. Universal sensing of ammonia gas by family of lead halide perovskites based on paper sensors: Experiment and molecular dynamics [J]. Materials Research Bulletin, 2021, 136: 111142.

[16] Li G., Zhang Y., Lin J., Xu X., Liu S., Fang J., Jing C., Chu J. Anomalous NH_3-induced resistance enhancement in halide perovskite $MAPbI_3$ film and gas sensing performance [J]. The Journal of Physical Chemistry Letters, 2021: 11339-11345.

[17] Jiao W., He J., Zhang L. Fabrication and investigation of a new all-inorganic lead free perovskite $Cs_3Bi_2I_6Br_3$ for ammonia detection at room temperature [J]. Journal of Alloys and Compounds, 2022, 895.

[18] Markina D. I., Anoshkin S. S., Masharin M. A., Khubezhov S. A., Tzibizov I., Dolgintsev D., Terterov I. N., Makarov S. V., Pushkarev A. P. Perovskite nanowire laser for hydrogen chloride gas sensing [J]. ACS Nano, 2023, (17): 1570−1582.